UDK 691.714:621.791
Original scientific article/Izvirni znanstveni članek

ISSN 1580-2949
Mater. Tehnol.

STRESS ANALYSIS AND NUMERICAL SIMULATION STUDY OF COLD METAL TRANSFER WELD HEAD

NAPETOSTNA ANALIZA IN ŠTUDIJ NUMERIČNE SIMULACIJE VARJENJA S POSTOPKOM PRENOSA KAPLJIC KOVINE NA HLADNO MESTO ZVARA

Mei Li, Fu Yang, Xiaolong Wei, Zheng Jia*

College of mechanical engineering, Shenyang University, Shenyang 110044, China

Prejem rokopisa – received: 2025-07-09; sprejem za objavo – accepted for publication: 2026-01-22

doi:10.17222/mit.2025.1520

In order to study stress and deformation during welding, the macroscopic and microscopic morphologies of the welded joints were recorded to obtain the best welding parameters. Taking a Q235 steel plate as the specimen, six groups were welded under different welding parameters using the cold metal transfer method. The stress field and deformation field in the welding process were simulated using the finite element method. The simulation results were used to further explain the experimental findings and to compare them with the experimental data. The results show that an excessive welding current aggravates the stress concentration of the joint and reduces the fatigue strength of the joint. If the welding current is too small, the stress of the base metal after welding is small, and there are defects including incomplete penetration and undercut. By comparison, the optimal welding parameters are identified as a current of 180 A, a voltage of 14.0 V, a welding speed of 600 mm/min, and a wire feeding speed of 5.5 m/min, under which good weld formation is achieved, and both stress and deformation are relatively low. The experimental results are basically consistent with the numerical simulation results.

Keywords: cold metal transfer welding, Q235 steel plate, stress analysis, numerical simulation, weld parameter

Avtorji članka so preučevali napetosti in deformacije nastale med varjenjem izbranega jekla vrste Q235. Zato, da bi ugotovili najboljše parametre varjenja so beležili makroskopske in mikroskopske morfologije zvarnih spojev. Objekt raziskave, opisane v tem članku, sta bili jekleni plošči iz Q235, ki so ju medsebojno spajali s postopkom varjenja pri katerem so uporabili metodo prenašanja kapljic kovine na hladno mesto zvara (angl.: cold metal transfer welding method) v obliki črke **V**. Uporabili so šest skupin različnih parametrov varjenja. S pomočjo metode končnih elementov so izvedli simulacije nastalih napetostnih in deformacijskih polj med varilnim procesom. Rezultate simulacije so avtorji uporabili za nadaljnjo razlago in primerjavo z eksperimentalnimi rezultati. Rezultati raziskave so pokazali, da prevelik varilni tok poveča koncentracijo napetosti v spoju in tako zmanjša dinamično trajno trdnost spoja. Če pa je varilni tok premajhen, je trdnost osnovne kovine po varjenju premajhna zaradi napak, ki so nastale kot posledica nepopolne penetracije raztaljene kovine v zvarni spoj in podrez. Primerjava med posameznimi parametri varjenja je pokazala, da so optimalni parametri varjenja za dobro oblikovan zvar ter relativno majhne notranje zaostale napetosti in deformacije naslednji: tok 180 A, hitrost varjenja 600 mm/min in hitrost podajanja žice 5,5 m/min. Eksperimentalni rezultati so se v osnovi dobro ujemali z rezultati numerične simulacije.

Ključne besede: postopek varjenja s prenosom kapljic kovine na hladno mesto zvara, jeklena pločevina tipa Q235, napetostna analiza, numerična simulacija, parametri varjenja

1 INTRODUCTION

Since the 20th century, welding technology has undergone extensive development and widespread application worldwide. Traditional MIG/MAG welding and CO_2 shielded welding have been widely used in industrial production due to their high welding efficiency, flexible welding positions, low cost, and low energy consumption.[1–6] However, due to their high heat input and significant deformation, welding under certain special conditions is severely limited.[7,8] CMT welding is a novel cold metal transfer technology. By precisely controlling the arc and molten pool during welding, it optimizes the welding heat input, thereby achieving better welding quality and formation.[9–11] Due to its high efficiency and stability, CMT welding technology has been widely applied to various metallic materials. For instance, it plays an important role in aerospace, automotive manufacturing, and precision instruments.[12–15] With the continuous development and innovation of welding technology, CMT welding will also be promoted and applied in more fields and applications. To improve welding efficiency and joint quality, in 2017, Wang Chong, Wang Shengkun et al.[16] from the China University of Petroleum used the ABAQUS numerical simulation method to study the expansion deformation rules and internal residual stress changes under different temperatures, large expansion ratios, and different expansion cone angles. They found that as the temperature increased, the maximum residual stress difference between the two materials gradually decreased. When the cone angle increased, the residual stress at the joint increased. In 2021, M. Saber[17] developed a ring expansion testing method to measure the

*Corresponding author's e-mail:
jz140@163.com (Zheng Jia)

hoop residual stress in thin-walled circular tubes. Through finite element simulation, the variation law of tube wall hoop residual stress with respect to the number of mandrels was derived. In 2022, Professor Zhang Jianbing[18] used the finite element method to conduct nonlinear numerical simulation research on casing expansion under different expansion tube cone angles. It was found that under different expander cone angles, residual tensile stress is observed on the inner wall of the tube, while residual compressive stress dominates the outer wall. Moreover, as the compressive force increased, the tool's taper and residual tensile stress also showed a linear relationship. Currently, both CMT and conventional arc welding have their own limitations. CMT equipment, processes, and weldability still require more in-depth research.[19–21] Q235, as a common steel, is widely used in industries such as construction, automotive, petrochemical, and aerospace sectors.[22] However, some issues, such as weld fracture and even detachment, have been observed in the welds produced using the CMT process in some enterprises.[23–25] Consequently, this study uses a THQ-50C wire as the welding material and employs CMT technology to weld Q235 steel plates. The effects of welding current, voltage, and wire feeding speed on weld formation are studied to obtain high-quality welded joints with excellent mechanical properties.

2 EXPERIMENTAL MATERIALS AND METHODS

2.1 Experimental materials and equipment

A THQ-50C low-carbon steel welding wire with a diameter of 1.2 mm was used. The base plate was Q235 steel with dimensions of (200 × 60 × 50) mm. The chemical compositions and mechanical properties of the wire and steel plate are shown in **Table 1** and **Table 2**, respectively. Ar 80 % + CO_2 20 % was used as the shielding gas with a flow rate of 18 L/min. A butt joint configuration was employed with a V-groove preparation: groove thickness of 5 mm, groove angle of 75°. A schematic diagram of the V-groove is shown in **Figure 1**. The equipment used in this experiment was a TransPuls Synergic 3200 CMT welding machine produced by Fronius International GmbH, Austria, and a CML-1016 stress tester.

Table 1: Chemical compositions of the THQ-50C wire and Q235 steel plate (*w*/%)

Material	C	Mn	Si	S	P
THQ-50C	0.06–0.15	1.40–1.85	0.80–1.15	≤0.035	≤0.025
Q235	0.12–0.22	≤1.40	≤0.35	≤0.05	≤0.045

Table 2: Mechanical properties of the THQ-50C wire and Q235 steel plate

Material	Tensile strength, MPa	Yield strength, MPa	Elongation, %
THQ-50C	≥500	≥420	≥22
Q235	375–500	235	≥26

2.2 Experimental methods

The prepared Q235 steel plates were first polished to remove rust. Then, TIG welding was used with a welding current of 150 A and a gas flow rate of 18 L/min to tack both weld ends of the polished base metal. The base metal was then fixed to the test bench using fixtures. The welding process parameters and trajectory were adjusted on the CMT computer interface to find the optimal welding angle and position. Subsequently, longitudinal weld beads were deposited at the butt joint of the base metal using the CMT welding machine under the six different sets of welding parameters selected in **Table 3**. After the welded base metal cooled down, the distances and angles between punch marks were measured and recorded. Resistance strain gauges were firmly glued to each measurement point on the base metal as shown in **Figure 2** and allowed to dry. Each strain gauge on the base metal was connected to the circuit of a resistance strain gauge instrument with a pre-adjusted balance box. The strain data from each strain gauge on the joint base metal was measured and recorded using the resistance strain gauge instrument. The stress and deformation trends of the weld were compared and evaluated to select the optimal parameters. Simulation software was then used to simulate and calculate the stress distribution of the weld, identifying the stress concentration zones, and the results were compared and analyzed with the experimental results. The deformation calculation formula and stress measurement steps are as follows:

Calculate the transverse deformation (b) (average value) at each measurement point: positive value indicates elongation, negative value indicates shortening, as shown in **Table 4**.

$$b = \frac{(b_1 - b_0) + (b_1' - b_0')}{2} \tag{1}$$

Where:

(b) – Transverse deformation

(b0) – Distance between front-side punch marks before welding

(b0') – Distance between back-side punch marks before welding

(b1) – Distance between front-side punch marks after welding

(b1') – Distance between back-side punch marks after welding

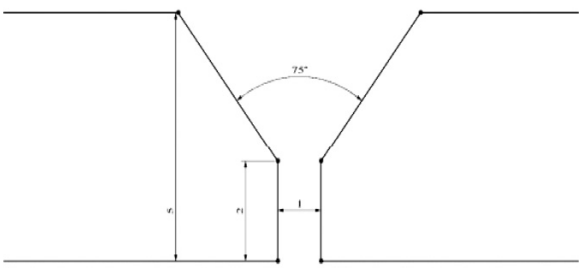

Figure 1: V-bevel

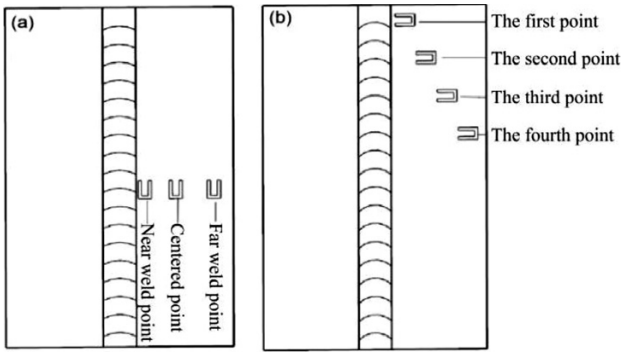

Figure 2: Strain gauge distribution: a) measuring transverse residual stress, b) measuring longitudinal residual stress

Plot the transverse deformation at each point along the length direction of the test plate.

Calculate the angular distortion (a), as shown in **Table 5**.

$$a = a_1 - a_0 \tag{2}$$

Where:

(a) – Angular distortion between punch marks

(a1) – Angle between punch marks before welding

(4) By measuring the stress at test point 1 (near the weld), test point 2 (midpoint), and test point 3 (far from the weld) along the X-direction of the post-weld material, the stress values at each point along the X-direction are obtained (**Table 4**). Similarly, by measuring the stress at four points along the Y-direction of the post-weld material from near to far from the weld, the stress values at each point along the Y-direction are obtained (**Table 5**). The data is then organized and plotted into **Figure 3** to observe the variation in stress values.

Table 3: Experimental parameters

Group No	Current, A	Voltage, V	Wire feeding speed, m/min	Welding speed, mm/min
Group 1	100	11.2	2.2	600
Group 2	160	13.6	4.8	600
Group 3	180	14.0	5.5	600
Group 4	200	14.3	6.4	600
Group 5	220	14.8	7.1	600
Group 6	240	16.2	7.9	600

3 EXPERIMENTAL RESULTS AND ANALYSIS

3.1 Welding joint stress analysis

From the stress values measured at each point in the X- and Y-directions (**Table 4** and **Table 5**), it can be seen that for Group 1, stress is mainly concentrated in the edge region of the base metal, where deformation is significant. For Groups 2 and 3, deformation in the weld zone is relatively small. For Groups 4, 5, and 6, weld stress is high, and deformation in the weld zone is relatively large. The stress distribution trend graphs plotted based on the stress values from **Tables 4** and **5** are shown in **Figure 3**.

Table 4: Stress values at each point in the X-direction (MPa)

Measuring point/item	1	2	3
Group 1	10	–10	–141
Group 2	234	295	–141
Group 3	223	268	–61
Group 4	230	273	–52
Group 5	229	273	–43
Group 6	244	300	–211

Table 5: Stress values at each point in the Y-direction (MPa)

Measuring point/item	1	2	3	4
Group 1	132	–93	–63	–105
Group 2	131	53	–135	–149
Group 3	138	68	–134	–151
Group 4	137	70	–135	–153
Group 5	144	78	–134	–152
Group 6	145	81	–131	–151

Comprehensively analyzing the X-direction and Y-direction stress distribution trends in **Figure 3**, Group 1 ex-

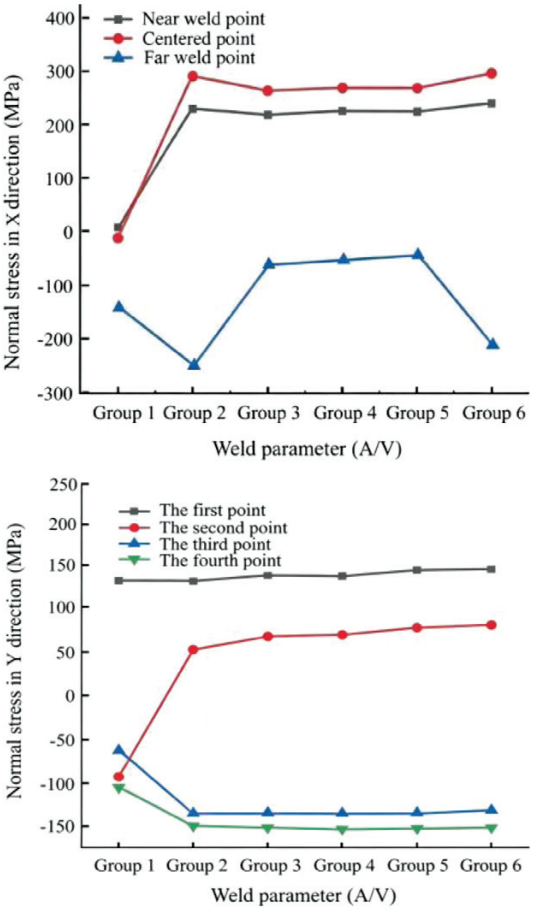

Figure 3: Trend of stress distribution: a) in the X-direction, b) in the Y-direction

hibits relatively small post-weld stress, while Groups 4, 5, and 6 show large stress distributions in the base metal after welding. Comparing the X and Y stress distribution trend graphs, the optimal welding parameters correspond to Group 3. Based on the comparison of pre- and post-weld stress measurements and weld formation, the welding currents of Groups 5 and 6 are excessive, resulting in high post-weld stress and significant deformation, as shown in **Figure 3** and **Tables 4–8**, and are therefore not optimal parameters. The absolute value of normal stress in the X-direction for Group 1 weld is too large, indicating excessive residual stress. Group 3 exhibits good weld formation with relatively small deformation and stress in the base metal after welding, making it the optimal parameter. From **Tables 6** and **7**, it can be seen that the transverse and longitudinal deformations of welds in Groups 4, 5, and 6 are large, while those in Groups 1, 2, and 3 are small. **Table 8** shows that the angular distortion in Groups 4, 5, and 6 is large, while it is small in Groups 1, 2, and 3.

Table 6: Welding transverse shrinkage deformation

Group/ Punch mark	1	2	3	4	5	6
Group 1	–0.19	–0.19	–0.15	–0.02	–0.02	–0.15
Group 2	–0.18	–0.29	–0.37	–0.47	–0.79	–0.38
Group 3	0.34	–0.2	0.06	–0.83	–0.14	–0.55
Group 4	0.94	0.64	0.87	0.40	0.20	0.60
Group 5	–1.64	–1.38	–1.46	–1.27	–1.13	–0.97
Group 6	–0.38	–0.26	–1.02	–0.23	–0.87	–0.51

Table 7: Welding longitudinal shrinkage deformation records (mm)

Group	Pre-weld L_0, mm	Post-weld L_1, mm
Group 1	200.08	199.86
Group 2	200.12	198.94
Group 3	200.04	198.34
Group 4	200.14	198.46
Group 5	200.02	198.22
Group 6	200.16	198.26

Table 8: Welding longitudinal shrinkage deformation records (°)

Group	1	2
Group 1	0.85	1.12
Group 2	0.87	1.15
Group 3	0.88	1.22
Group 4	2.70	3.10
Group 5	3.80	3.90
Group 6	3.96	4.02

To study the deformation of Q235 steel plate after butt welding, welding experiments were conducted using the six groups of CMT experimental data, mainly considering the out-of-plane deformation of the weldment. The results are shown in **Figure 4**.

From **Figure 4**, it can be observed that during the experiment, the weld under a current of 100 A and a voltage of 11.2 V exhibited defects such as undercut. The welds under a current of 220 A and a voltage of 14.8 V as well as a current of 240 A and a voltage of 16.2 V had large heat-affected zones, stress concentration, and severe deformation, indicating they are not optimal param-

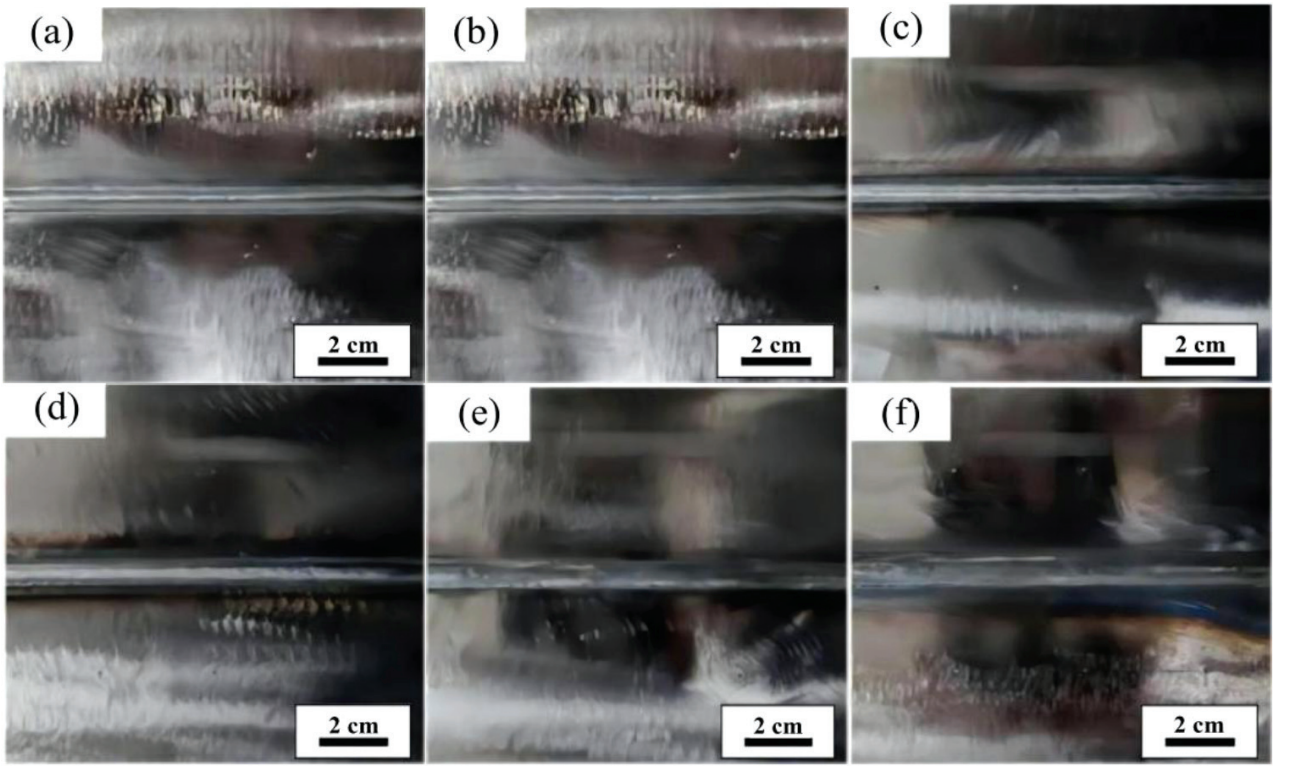

Figure 4: Butt joint results: a) 100 A, 11.2 V; b) 160 A, 13.6 V; c) 180 A, 14.0 V; d) 200 A, 14.3 V; e) 220 A, 14.8 V; f) 240 A, 16.2 V

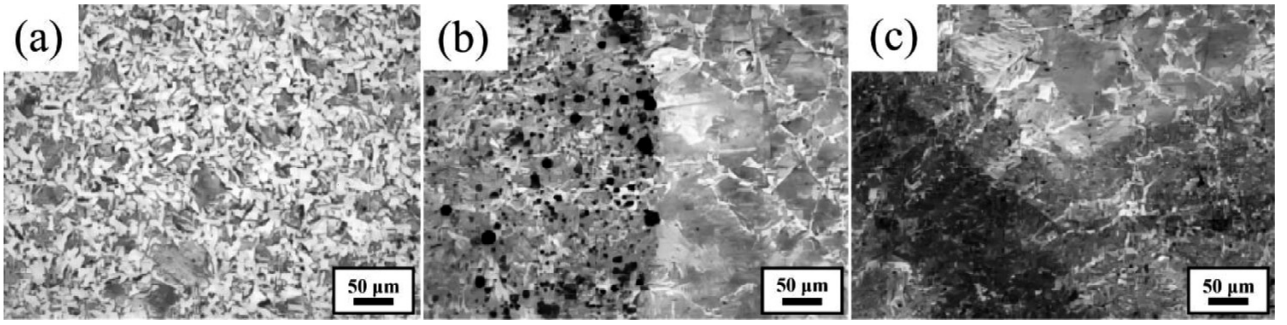

Figure 5: Butt joint metallographic structure: a) base metal microstructure of the butt joint; b) butt joint microstructure at 180 A, 14.0 V; c) butt joint microstructure at 220 A, 14.8 V

eters. The weld under a current of 180 A and a voltage 14.0 V exhibited good formation with relatively low stress. Therefore, these parameters represent the optimal CMT welding parameters for Q235 steel plate.

3.2 Joint microstructure analysis

Microstructural observation was performed on butt joints, as shown in **Figure 5**. **Figure 5a** shows the metallographic structure of the base metal in the Q235 steel CMT butt joint. The internal microstructure of the material can be observed, primarily composed of ferrite and pearlite. The brighter areas represent ferrite, exhibiting a polygonal morphology with good ductility and toughness. The darker lamellar areas are pearlite, composed of ferrite and cementite (Fe_3C), providing strength to the material. Ferrite provides good plasticity and toughness, while pearlite enhances the material's strength and hardness. Due to its low heat input, CMT welding helps form a fine and uniform grain structure, thereby improving the mechanical properties of the welded joint as well as reducing welding stress and deformation. This microstructure enables the Q235 welded joint to exhibit excellent comprehensive mechanical properties under different stress states.

The metallographic structure of the butt joint under 180 A current is shown in **Figure 5b**. The weld metal zone (left) exhibits a fine grain structure with a small amount of porosity and inclusions. The fine grain structure results from the low CMT heat input, enhancing the strength and toughness of the weld. The base metal zone (right) shows a typical ferrite and pearlite structure with larger grains. Microstructural characteristics directly affect the mechanical properties of the joint. The fine, uniform grain structure in the weld zone enhances tensile strength and yield strength. In contrast, the large grains in the base metal zone provide plasticity, ensuring that no brittle fracture occurs under external forces.

The metallographic structure of the Q235 butt joint obtained with CMT welding under a current of 220 A is shown in **Figure 5c**. The weld zone exhibits a relatively coarse grain structure. A distinct weld metal zone and base metal zone can be observed. The grains in the weld zone are coarse and unevenly distributed, indicating that high current caused significant thermal effects, grain growth, and coarsening, leading to a decrease in elongation. Additionally, there may be more porosity and inclusions in the weld zone, further weakening the overall material performance. Therefore, 180 A and 14.0 V represent the optimal CMT welding parameters for the Q235 steel plate.

Based on the experimental results, it is understood that the stress and deformation generated during welding have various negative impacts on the manufacturing precision and strength performance of welded structures. To improve welding quality, it is necessary to take certain measures to optimize weld formation. Generally, methods to reduce welding deformation include the following aspects:

Careful design is the key to reducing welding deformation and ensuring that the component cross-section is as symmetrical as possible. Generally, reasonable arrangement of weld positions, reducing the number of welds, decreasing the weld cross-sectional area, and selecting appropriate groove forms can effectively reduce welding deformation.

(2) In practical applications, selecting appropriate heat input is crucial. As the input heat increases, weld deformation also increases. Multi-pass welding at low current is usually adopted instead of single-pass welding. Using techniques like backstep welding, staggered welding, and segmented symmetric welding to replace continuous welding prone to deformation can effectively reduce welding deformation. Selecting suitable welding processes can effectively optimize weld formation.

(3) Pre-deformation is a commonly used technique to effectively optimize weld formation. Pre-deformation involves preparing the workpiece before welding based on the experience of on-site workers. The applied deformation should be opposite to that produced during welding, thereby offsetting part of the welding deformation.

4 SIMULATION OF THE Q235 STEEL PLATE BUTT JOINT EXPERIMENT

The simulation software provided two heat source models: a three-dimensional Gaussian volumetric heat source and a Gaussian surface heat source. The numerical simulation software has two solvers, both being finite

element solvers incorporating heat conduction and deformation, with strong nonlinear capabilities and material property functions.

To further explain the experimental results, a welding simulation model was developed in a Windows environment. The weld was modeled using a process tree-based method to simulate the stress changes and deformation caused by the butt joint of the Q235 steel plate. In the welding numerical simulation, a mesh model was first established, the weld and material models were defined, and welding conditions were set, i.e., pre-processed. The simulation was performed in accordance with the conditions set during pre-processing. The calculated stress field and welding deformation results are shown in **Figures 6–11**.

(1) Numerical simulation of total deformation under different welding parameters

The contour plot of total deformation distribution for the joint (**Figure 6**) shows that larger parameters result in larger deformation concentrated in the weld zone. Deformation in the weld zone is relatively small for (a), (b), (c); deformation is excessive for (d), (e), (f).

(2) Numerical simulation of the X-axis deformation component under different welding parameters

The contour plot of X-axis deformation component distribution for the joint (**Figure 7**) shows that for (a) stress is mainly concentrated in the edge region of the base metal, where deformation is significant; for (b), (c) deformation in the weld zone is relatively small; for (d), (e), (f) weld stress is high, and deformation in the weld zone is relatively large.

(3) Numerical simulation of the Y-axis deformation component under different welding parameters

The contour plot of Y-axis deformation component distribution for the joint (**Figure 8**) shows that for (a) deformation is large at the top of the base metal in the positive Y-direction, corresponding to the weld start segment; for (b), (c) deformation in the weld zone is small; for (d), (e), (f), deformation in the weld zone is large.

(4) Numerical simulation of equivalent stress under different welding parameters

The contour plot of equivalent stress distribution for the joint (**Figure 9**) shows that larger parameters result in higher equivalent stress concentrated in the weld zone.

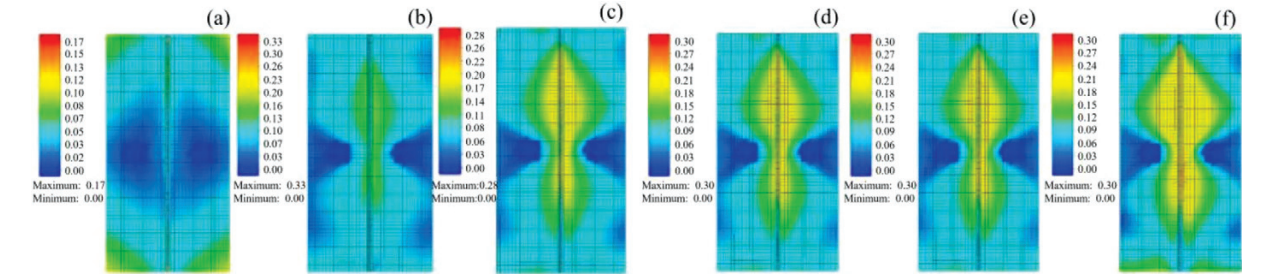

Figure 6: Numerical simulation of total deformation under different welding parameters: a) 100 A, 11.2 V; b) 160 A, 13.6 V; c) 180 A, 14.0 V; d) 200 A, 14.3 V; e) 220 A, 14.8 V; f) 240 A, 16.2 V

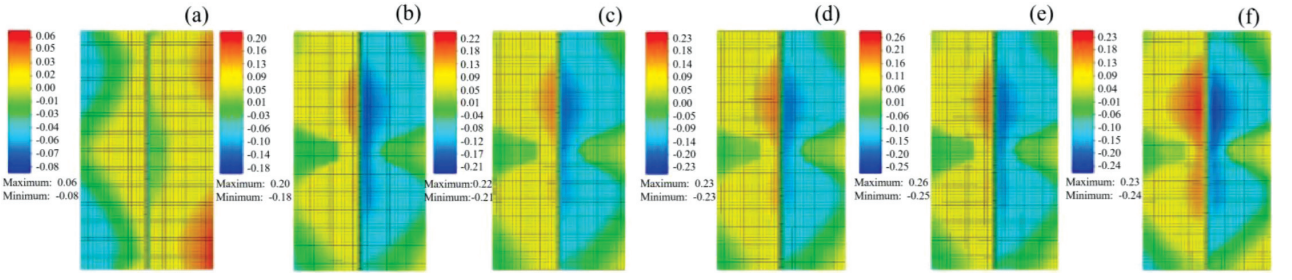

Figure 7: Numerical simulation of X-axis deformation component under different welding parameters: a) 100 A, 11.2 V; b) 160 A, 13.6 V; c) 180 A, 14.0 V; d) 200 A, 14.3 V; e) 220 A, 14.8 V; f) 240 A, 16.2 V

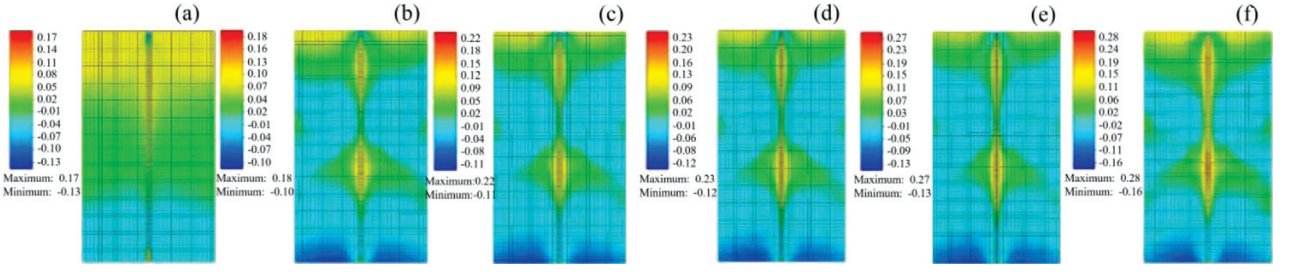

Figure 8: Numerical simulation of Y-axis deformation component under different welding parameters: a) 100 A, 11.2 V; b) 160 A, 13.6 V; c) 180 A, 14.0 V; d) 200 A, 14.3 V; e) 220 A, 14.8 V; f) 240 A, 16.2 V

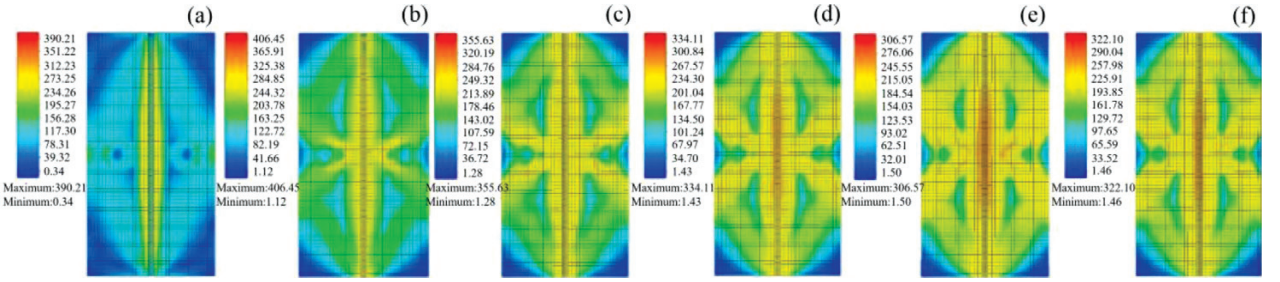

Figure 9: Numerical simulation of equivalent stress under different welding parameters: a) 100 A, 11.2 V; b) 160 A, 13.6 V; c) 180 A, 14.0 V; d) 200 A, 14.3 V; e) 220 A, 14.8 V; f) 240 A, 16.2 V

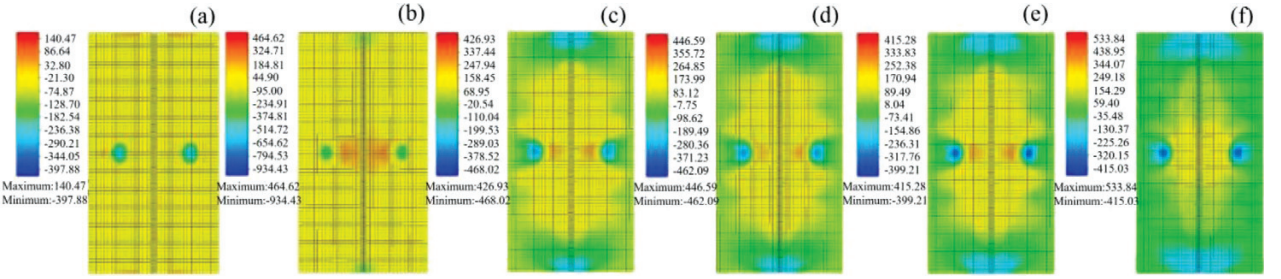

Figure 10: Numerical simulation of X-direction normal stress component under different welding parameters: a) 100 A, 11.2 V; b) 160 A, 13.6 V; c) 180 A, 14.0 V; d) 200 A, 14.3 V; e) 220 A, 14.8 V; f) 240 A, 16.2 V

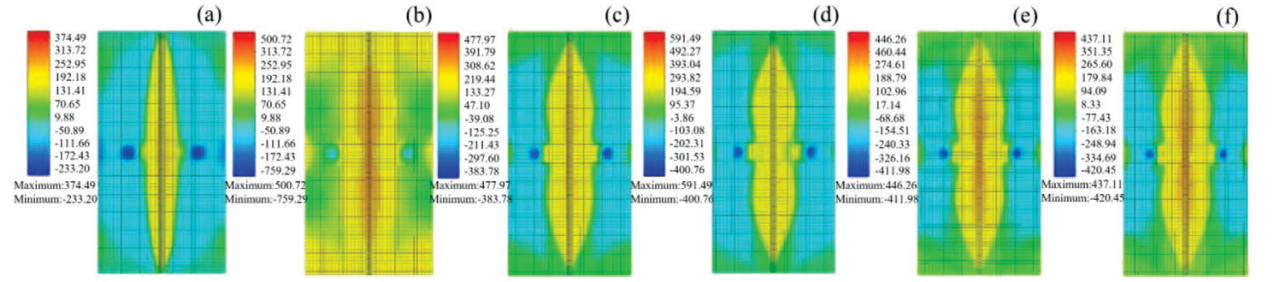

Figure 11: Numerical simulation of Y-direction normal stress component under different welding parameters: a) 100 A, 11.2 V; b) 160 A, 13.6 V; c) 180 A, 14.0 V; d) 200 A, 14.3 V; e) 220 A, 14.8 V; f) 240 A, 16.2 V

Equivalent stress in the weld zone is relatively small for (a), (b), (c); stress is excessive for (d), (e), (f), significantly affecting mechanical properties, so these three groups are not ideal parameters.

(5) Numerical simulation of X-direction normal stress component under different welding parameters

The contour plot of X-direction normal stress component distribution (**Figure 10**) shows that larger parameters result in higher equivalent stress concentrated in the weld zone. Equivalent stress in the weld zone is relatively small for (a), (b), (c); stress is excessive for (d), (e), (f).

(6) Numerical simulation of Y-direction normal stress component under different welding parameters

The contour plot of Y-direction normal stress component distribution (**Figure 11**) shows that larger parameters result in higher equivalent stress concentrated in the weld zone. Equivalent stress in the weld zone is relatively small for (a), (c); stress is excessive for (b), (d), (e), (f).

From the above simulation results, it can be seen that (d), (e), (f) generate large equivalent stress in the weld zone and the base metal adjacent to the heat-affected zone (HAZ), with relatively large post-weld deformation; (a), (b) generate relatively small equivalent stress in the weld zone and adjacent HAZ base metal, with small deformation; (c) represents the condition with pre-deformation (counteracting deformation), exhibiting the optimal stress parameters.

5 Conclusions

This paper analyzed the deformation and stress distribution trends of CMT butt-welded joints of Q235 steel plates under different currents and voltages using experimental and numerical simulation methods. By comparing simulation software calculations with experimental measurements, the following conclusions were obtained:

(1) Comparing the simulation results of the butt joint with the actual experimental results, it is found that the simulated stress field and welding deformation are consistent with the experimental results. During the experiment, it was found that welds formed under a current of 100 A, a voltage of 11.2 V, a welding speed of

600 mm/min, and a wire feeding speed of 5.5 m/min exhibited defects such as undercut. During measurement, it was found that welds with a current of 220 A, a voltage of 14.8 V, a welding speed of 600 mm/min, a wire feeding speed of 5.5 m/min, as well as a current of 240 A, a voltage of 16.2 V, a welding speed of 600 mm/min, and a wire feeding speed of 5.5 m/min exhibited large heat-affected zones, stress concentration, and severe deformation, indicating that these are not optimal welding parameters. Both experimental and simulation results show that the weld formed under a current of 180 A, a voltage of 14.0 V, a welding speed of 600 mm/min, a wire feeding speed of 5.5 m/min, and a base metal thickness of 5 mm exhibits good formation with relatively low stress. Therefore, these parameters represent the optimal CMT options for the Q235 steel plate.

(2) Through experimental and simulation results, it can be seen that excessively high current parameters lead to intensified stress concentration at the joint, thereby reducing the fatigue strength of the joint. Although excessively low parameters result in small stress in the base metal after welding, defects such as incomplete penetration and undercut occur.

(3) The post-weld stress distribution and deformation were determined through experimental measurements and finite element calculations. By studying six groups of experiments with different parameters and the finite element model, the optimal pre-deformation and stress parameters were established as 180 A, 14.0 V, a welding speed of 600 mm/min, and a wire feeding speed of 5.5 m/min. The calculation results show good weld formation and low stress values for the base metal surface.

Acknowledgements

The authors acknowledge the financial support from the Key Project of the Education Department of Liaoning Province [LJKZ1171].

6 REFERENCES

[1] C. H. Wang, P. Y. Wang, S. Q. Chu, et al., Effect of CMT+P Welding Current on Microstructure and Mechanical Properties of 5083 Aluminum Alloy Welded Joints, Material Development and Application, 37 (**2022**) 04, 71–76, doi:10.19515/j.cnki.1003-1545.2022.04.001

[2] Y. H. Sun, Y. Z. Liu, C. J. Luan, et al., The effect of welding heat input on the structure and properties of CMT backing welding joint, Metal Processing (hot working), 11 (**2023**), 22–26

[3] M. Liu, Study on technology and mechanical properties of joint of dissimilar AZ31B Mg/6061 Al alloys by CMT welding, Zhenjiang: Jiangsu University of Science and Technology, 2017

[4] H. K. Yuan, B. Q. Wei, T. K. Guo, et al., Comparison of Aluminum Alloy Welding Quality Between CMT and MIG, Aluminum Processing, 01 (**2018**), 56–60

[5] Q. I. Chu, Q. L. Cao, Z. G. Xie, et al., Microstructure and Properties of 1J50 and 0Cr18Ni9 Welding Joints under Different Welding Methods, Welded Tube, 46 (**2023**) 10, 21–27, doi:10.19291/j.cnki.1001-3938.2023.10.004

[6] C. Zhang. Study on microstructure and properties of Al alloy and steel CMT welding-brazing, Zhenjiang: Jiangsu University of Science and Technology, 2024

[7] Q. L. Meng, Study on the Welding Process of Stainless Steel Sheet by Cold Metal Transfer (CMT), Changchun: Jilin University, 2015

[8] S. Luo, Z. Wu, D. Wang, et al., Solidification microstructures and softening behavior of laser welded 6082-A356 aluminum alloy dissimilar butt joints, Materials Today Communications, 38 (**2024**), 108411–108413

[9] T. Kuboki, K. Nishida, T. Sakaki, et al., Effect of plug on levelling of residual stress in tube drawing, Journal of Materials Processing Technology, 204 (**2008**) 1, 162–168

[10] Y. K. Kim, M. H. Song, Effects of expanding methods on residual stress of expansion transition area in steam generator tube of nuclear power plants, Academic Conference of Korea Energy Society, 21 (**2012**) 4, 362–372

[11] Y. F. Zhang, D. J. Li, Y. Xiong, et al., Analysis on difference of collapse strength of two kinds of expansion tubes after expansion, Journal of Material Heat Treatment, 43 (**2022**) 11, 190–196, doi:10.13289/j.issn.1009-6264.2022-0179

[12] G. Mu, Interfacial organization regulation and properties of CMT welded joints made of TC4/304L dissimilar materials, Shanghai: Shanghai Jiao Tong University, 2022

[13] X. Zhang, Study on microstructure and properties of CMT additive repair of 2A12 aluminum alloy, Nanchang: Nanchang Aviation University, 2022

[14] Y. Han Y, S. Zhong, L. Tian, et al., Welding heat input for synergistic improvement in toughness and stress corrosion resistance of X65 pipeline steel with pre-strain, Corrosion Science, 206 (**2022**), 1–15

[15] Y. Han, S. Zhong, C. Peng, et al., Fatigue behavior of X65 pipeline steel welded joints prepared by CMT/GMAW backing process, International Journal of Fatigue, 164 (**2022**), 1–14

[16] C. Wang, S. K. Wang, S. G. Xu, Effect of forming temperature on strength of monohole expandable tubular with thread connection, Journal of Plastic Engineering, 24 (**2017**) 03, 50–56

[17] M. Saber, H. Chouikhi, Development of the bicone mandrel ring expansion test to evaluate the hoop stress in extruded aluminum tubes, Experimental Mechanics, 61 (**2021**) 2, 791–802

[18] J. B. Zhang, D. T. Kong, C. Y. Jiang, et al., Effect of tool cone angle on circumferential residual stress of expansion casing, Journal of Plastic Engineering, 29 (**2022**) 01, 155–161

[19] J. Poduska, J. Kucera, P. Hutar, et al., The Effect of Specimen Size on the Determination of Residual Stress in Polymer Pipe Wall, Key Engineering Materials, 627 (**2014**), 141–144

[20] T. Wojdat, P. Kustron, A. Margielewska, M. Stachowicz, Microstructure and Mechanical Properties of Braze Welded Joints of Copper with Austenitic Steel Made by CMT Method, Archives of Metallurgy and Materials, 64 (**2019**) 4, 1411–1420

[21] W. Z. Luo, H. M. Cheng, H. Y. Liu, et al., Numerical Simulation of Residual Stress and Welding Deformation for High Strength Steel Q960E Butt-welded Joints, China Mechanical Engineering, 34 (**2023**) 17, 2095–2105

[22] O. Muransky, C. J. Hamelin, M. C. Smith, et al., The effect of plasticity theory on predicted residual stress fields in numerical weld analyses, Computational Materials Science, 54 (**2012**), 125–134

[23] Y. Chen, Z. Yang, C. Shi, et al., Laser-CMT Hybrid Welding-Brazing of Al/Steel Butt Joint: Weld Formation, Intermetallic Compounds, and Mechanical Properties, Materials, 12 (**2019**) 22, 3651–3652

[24] C. Liu, Study on 2205 Duplex Stainless Steel with Twin-CMT Welding and Numerical Simulation, Chongqing: Chongqing Institute of Science and Technology, 2020

[25] Y. H. Zhu, Z. Q. Geng, Limitation of sheet metal welding—CMT cool metal transition technique, Electric Welding Machine, 41 (**2011**), 78–80 + 84